Dynamic stall for a Vertical Axis Wind Turbine in a two-dimensional study

R. Nobile[1,*], M. Vahdati[1], J. Barlow[1], A. Mewburn-Crook[2]

[1] *University of Reading, Reading, UK*
[2] *Wind Dam Renewables Ltd, Swansea, UK*
***** *Corresponding author. Tel: +44 1183784666, E-mail: r.nobile@reading.ac.uk*

Abstract: The last few years have proved that Vertical Axis Wind Turbines (VAWTs) are more suitable for urban areas than Horizontal Axis Wind Turbines (HAWTs). To date, very little has been published in this area to assess good performance and lifetime of VAWTs either in open or urban areas. At low tip speed ratios (TSRs<5), VAWTs are subjected to a phenomenon called 'dynamic stall'. This can really affect the fatigue life of a VAWT if it is not well understood. The purpose of this paper is to investigate how CFD is able to simulate the dynamic stall for 2-D flow around VAWT blades. During the numerical simulations different turbulence models were used and compared with the data available on the subject. In this numerical analysis the Shear Stress Transport (SST) turbulence model seems to predict the dynamic stall better than the other turbulence models available. The limitations of the study are that the simulations are based on a 2-D case with constant wind and rotational speeds instead of considering a 3-D case with variable wind speeds. This approach was necessary for having a numerical analysis at low computational cost and time. Consequently, in the future it is strongly suggested to develop a more sophisticated model that is a more realistic simulation of a dynamic stall in a three-dimensional VAWT.

Keywords: *Vertical Axis Wind Turbine (VAWT), Urban Area, Computational Fluid Dynamics (CFD), Dynamic Stall, Turbulence Model*

Nomenclature

N	*number of rotor blades*	λ	*tip speed ratio* $(\Omega R/ U_\infty)$
c	*airfoil/blade chord* ..... *mm*	θ	*azimuth angle* ..... *deg*
t	*thickness of the blade* ..... *mm*	α	*angle of attack* ..... *deg*
s	*span of the blade* ..... *mm*	V	*relative wind speed* ..... *m/s*
R_r	*radius of rotor* ..... *mm*	ω	*rotational speed* ..... *rad/s*
R_m	*radius of central mast* ..... *mm*	*PIV*	*Particle Image Velocimetry* .....
U_∞	*undisturbed velocity* ..... *m/s*	Ω	*rotation frequency/vorticity* ..... *rad/s*

1. Introduction

In the last few decades, the production of electricity from wind turbines has seen a rapid growth in many countries around the world. The major drivers are the recent need to reduce CO_2 emissions into the atmosphere and meet the growing demand for electricity [1]. One promising alternative for the future generation of electricity is the installation and integration of wind turbines in the built environment combined with other alternative sustainable systems [2], [3]. The benefits are mainly generation of electricity on the site where it is needed with reduction in transmission losses and cable costs [3].

In the late 1970s and early 1980s, very little research was conducted on V AWTs on understanding the aerodynamics and flow interaction between blades during the operation of a wind turbine [4]. Recently, the progress of small wind turbines in the built environment has been mainly focused on Horizontal Axis Wind Turbines (HAWTs) rather than Vertical Axis Wind Turbines (VAWTs). But several studies have shown that VAWTs are more suitable for urban areas than HAWTs [3], [5], [6], [7]. The advantages are mainly: omni-directional without a yaw control, better aesthetics to integrate into buildings, more efficient in turbulent environments and lower sound emissions [8]. In addition there is some research speculating

that VAWTs are appropriate for large scale of 10 MW or more, as VAWTs can operate mechanically better than HAWTs [9], [10]. They can withstand high winds due to their aerodynamic stall behaviour [5]. Generally, the aerodynamic analysis of a VAWT is very complicated, as the blades are called on to operate in unsteady flow, pitching relative to the mean flow and cutting the stream tube twice [5]. One important aspect to consider during the operation of a VAWT at low wind speeds is the generation of a phenomenon called dynamic stall. The phenomenon is mainly characterised by the development of vortices that will interact with the airfoil of the blades and have a substantial impact on the design and power generation of the wind turbine [11].

The main purpose of this work is to understand how ANSYS CFX 12.0 is able to approach the development of dynamic stall around the blades of a VAWT. Also, the final objective of the numerical study is to make a contribution in the field of dynamic stall as many straight-bladed VAWTs are called to operate. In this paper a number of simulations are explored to understand static and dynamic stall around the rotor of a 3 straight-bladed VAWT. To reduce time and memory costs a 2 -D case is explored for all numerical simulations. The Computational Fluid Dynamics (CFD) Software used was ANSYS CFX 12.0. Here, the three turbulence models analysed were the k-ε model, the standard k-ω model and the SST (Shear Stress Transport) model. The numerical simulations were studied for different tip speed ratios and compared with the small amount of experimental data available in literature.

2. Methodology

In order to understand the physics involved during dynamic stall of a straight-bladed vertical Darrieus wind turbine, a 2-D rotor is proposed and analysed. This 2-D approach is adopted for reducing time and computational costs. The airfoil analysed, for the VAWT, is a NACA 0018 and its characteristics are listed in Table 1. The rotor is composed of 3 blades and a central mast. The solid model of the rotor was generated with ProEngineer 4.0 and imported into ANSYS CFX 12.0.

Table 1: Properties of the rotor

NACA0018					
Cord c (mm)	Thickness t (mm)	Span s (mm)	Rotor Radius R_r (mm)	Number Blades N	Mast Radius R_m (mm)
490	88.2	50	3000	3	75

The mesh, as shown in Figure 1, is mainly composed of three sub-domains: one fixed sub-domain outside the rotor, one dynamic sub-domain around the blades of the rotor and one fixed sub-domain for the remaining part of the rotor. The mesh was generated by adopting a Sweep Method with one element deep and the total number of elements is 4.58×10^5, as listed in Table 2.

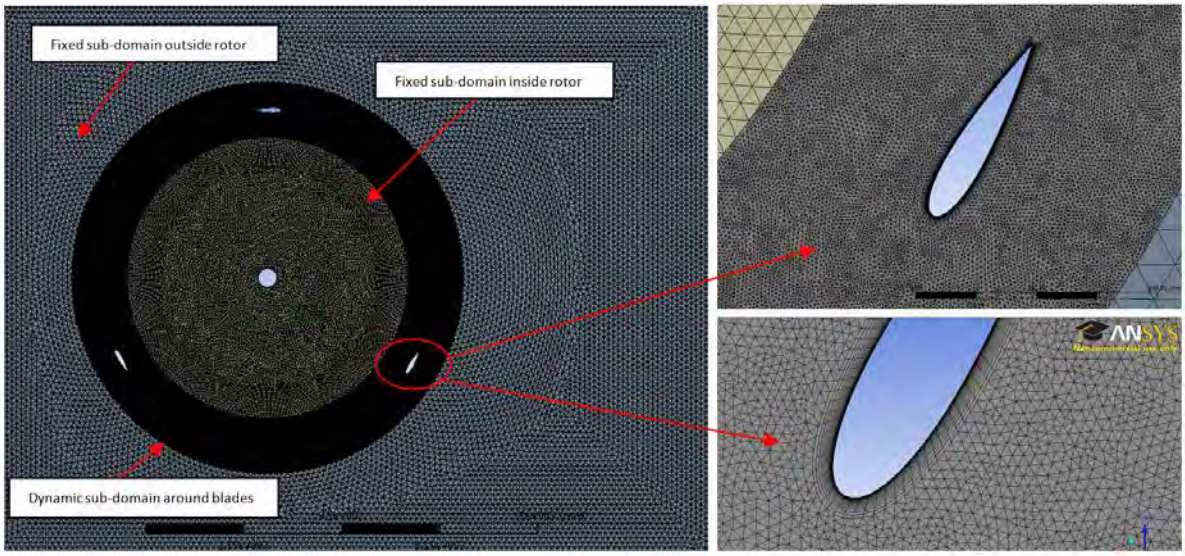

Fig. 1. Mesh for the 2-D rotor

Table 2. Sub-domain properties

Sub-domain	Number of elements
1) Fixed sub-domain outside rotor	$20*10^3$
2) Dynamic sub-domain around blades	$42*10^4$
3) Fixed sub-domain inside rotor	$18*10^3$
Total number of elements	$4.58*10^5$

All sub-domains were meshing by using only triangle elements, as they are more appropriate for simulations involved fluids [12]. The mesh around the blades of the rotor, which is a wake development region, was refined through the use of the facing sizing and inflation options available in ANSYS 12.0. In this region, the use of prism elements is able to capture boundary layer effects more effectively and efficiently. The three different meshes were linked together with the use of domain interfaces. Symmetrical boundaries were used for the top and bottom parts of the 2-D model with no-slip boundary conditions at the two sides. An opening boundary was chosen for the output and a constant wind speed of 6 m/s, with a turbulence intensity of 5%, was defined for the inlet. The two wall sides were placed at 4c from the diameter of the blades respectively. The outlet and inlet were placed 4c and 10c away respectively. Table 3 gives a summary of the parameters employed in the four different cases where different time steps and tip speed ratios (TSRs) were defined. For all transient simulations a total time was defined to give enough time for the flow to develop around the blades of the rotor. Finally, the residual target, in the convergence criteria, was set to be 10^{-4}.

Table 3. Input data for the four cases analysed

Simulation Case	Tip speed ratio	Angular speed (rad/s)	Time for one rotation (s)	Angle of attack (deg.)	Time Step Simulation (s)
Case 1	$\lambda_1=2.3$	$\omega_1=4.7$	$t_1=1.33$	$-30\leq\alpha_1\leq30$	0.0037
Case 2	$\lambda_2=3.0$	$\omega_2=6.0$	$t_2=1.05$	$-21\leq\alpha_1\leq21$	0.0029
Case 3	$\lambda_3=4.0$	$\omega_3=8.0$	$t_3=0.78$	$-15\leq\alpha_1\leq15$	0.0022
Case 4	$\lambda_4=5.0$	$\omega_4=10$	$t_4=0.63$	$-12\leq\alpha_1\leq12$	0.0017

The effect of different TSRs are presented and discussed in the conclusions section of this paper.

2.1. Dynamic Stall

Although VAWTs have several advantages over HAWTs, the aerodynamics around the blades is very complicated [11]. VAWTs, during their operation, are called to work under both static and dynamic stall conditions. Consequently, the blades are subjected to cyclic forces due to the variation of incidence angle of the blade relative to the wind direction [13]. Although the presence of dynamic stall at low TSRs can have a positive impact on the power generation of a wind turbine, the formation of vortices can generate other problems such as vibrations, noise and reduction of fatigue life of the blades due to unsteady forces [13]. Larsen et al. [14] show that dynamic stall is mainly characterised by flow separations at the suction side of the airfoil. This can be summarised in four crucial stages: 1) Leading edge separation starts, 2) Vortex build-up at the leading edge, 3) Detachment of the vortex from leading edge and build-up of trailing edge vortex, 4) Detachment of trailing edge vortex and breakdown of leading edge vortex. The sequence of these four flow events will generate unsteady lift, drag and pitching moment coefficients with a large range of flow hysteresis dependent on the angle of attack [15]. The expression of the angle of attack α adopted for the simulation, without induction factor, is given by Eq. (1):

$$\alpha = \arctan\left(\frac{\sin\theta}{\lambda - \cos\theta}\right) \tag{1}$$

where θ is the azimuth angle and λ the TSR. In this study, as shown in Table 3, four different cases are analysed with different parameters that are highly dependent on the TSRs.

2.2. Turbulence Models

Wang et al. [16] show that the most popular turbulence models, adopted in the CFD community, are mainly Direct Numerical Simulation (DNS), Large Eddy Simulation (LES) and Reynolds-Averaged Navier-Stokes (RANS). The DNS method today requires a large amount of computing resources and time. The LES method is more appropriate for 3-D simulations. Therefore, the only method adopted for this 2-D numerical study was the RANS method. The three RANS turbulence methods analysed, due to low computational costs, are: the standard k-ω model, the standard k-ε model and the SST model. A more detailed description about the turbulence methods can be found in the book by Wilcox [17].

3. Results

In this section of the paper a number of numerical simulations are analysed for different TSRs. The numerical simulations obtained during the present study are mainly compared with the study carried out by Wang et al. [16], as this previous numerical study showed a good agreement with experimental data. However, it should be point out few differences between the two numerical studies. The main differences are summarised and listed in Table 4.

In this numerical study, a number of cycles of the rotor were calculated at different TSRs until a periodic solution was achieved. The total time was set to be 4s to give enough time for the rotor to reach a period state in all four cases.

Table 4. Main differences between the two numerical methods

Present Study	Wang et al. Study
ANSYS CFX	FLUENT
Rotor with 3 blades and central mast	Single pitching blade
Free-stream turbulence intensity 5%	Free-stream turbulence intensity 0.25%
Variable time step with angular velocity	Constant time step
Triangle elements	Quadrilateral elements
$\alpha=\arctan(\sin\theta/\lambda-\cos\theta)$	$\alpha=10^0+15^0\sin(\omega t)$
Wake interactions	No wake interaction
No converged steady state	Initial input from converged steady state

In Fig. 2 and Fig. 3, the left side, show graphically the results obtained for this numerical analysis, while the right side compare the CFD results of Wang et al. with experimental data by Lee and Gerontakos [18]. Furthermore, Fig. 2 and 3 show how the lift and the drag coefficients, C_l and C_d, are affected by different angles of attack and TSRs. The curve shapes are in good agreement with the experimental data obtained by Lee and Gerontakos. Here, the final results are more realistic and less fluctuating than the CFD simulation conducted by Wang et al [16]. Also, a strong instability at high angles of attack is observed and is thought to be due to the deep dynamic stall that is typical for low TSRs. However, the few exceptions are the absence of a second peak on the curves due to the presence of a trailing edge vortex and the lack of intersection points between upstroke and downstroke paths that are seen in the experimental graphs on the right.

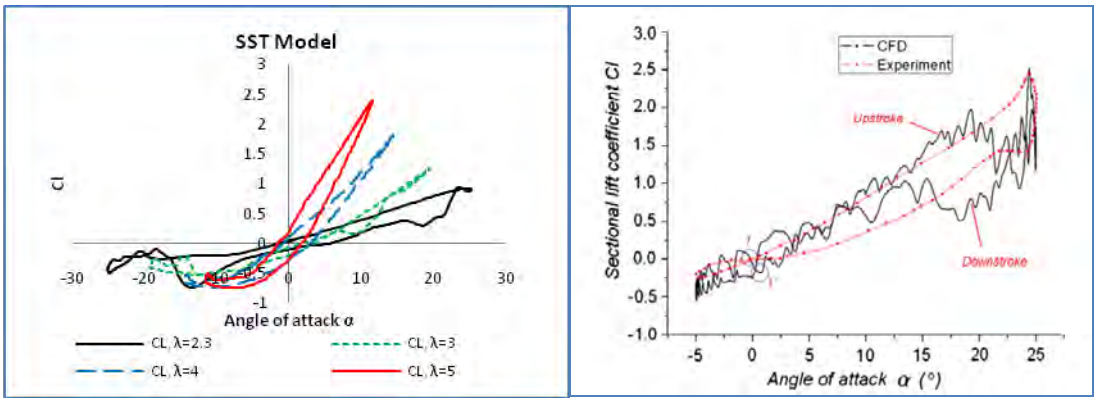

Fig. 2. Lift coefficient C_L for the two numerical studies and experimental data

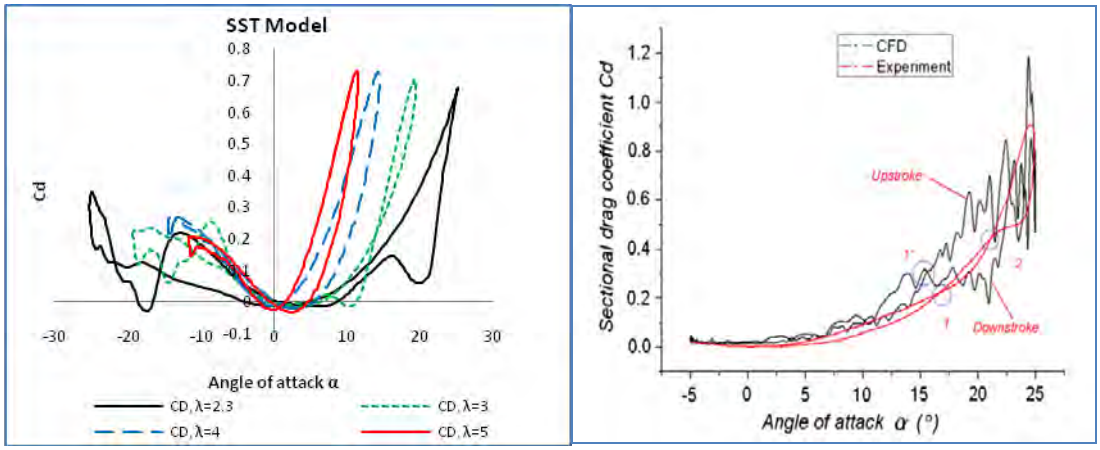

Fig. 3. Drag coefficient C_D for the two numerical studies and experimental data

However, the development of several peaks, especially for negative angle of attacks and low TSRs can be associated with the development of upstream wakes that will interact with the downstream blades. Also the presence of a central mast will generate several wakes that will affect the flow downstream. The different hysteresis loops in Fig. 2 and 3, show clearly the development of two phenomena called dynamic and static stall. Dynamic stall typically will develop at high angle of attacks for $\lambda<4$ and is characterised by its fluctuating nature, while static stall will take place at low angle of attacks for $\lambda \geq 4$ with smoother curves and less intersection points. One important consideration is that the range of angle of attack is different from the experimental data obtained by Lee and Gerontatos. This is mainly due to the use of Eq. (1) instead of using $\alpha=10^0+15^0\sin(\omega t)$ that is typically adopted for the case of a pitching motion single blade.

Finally, the numerical results are analysed by comparing the evolution of the shed vorticity with the experimental data available in the field of dynamic stall. Fig. 4 shows the vorticity field at $\theta=120^0$ for the three turbulence methods adopted in this numerical study. The SST method shows a good agreement with the experimental data obtained by Ferreira et al. [19] and Wang et al. [16] than the k-ω and k-ε methods that are more dissipative. This turbulence method is able to show the generation of specific vortices at the leading and trailing edges respectively. A more detailed explanation will be given in the next section for the SST method, as the results best agreeing with experiments

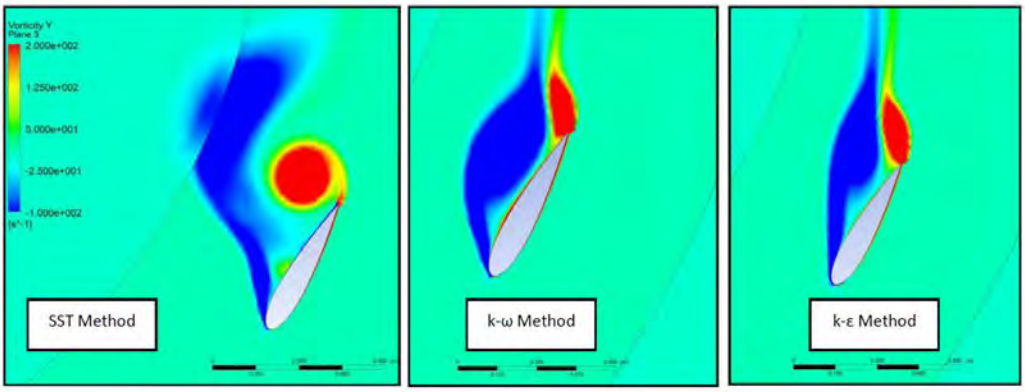

Fig. 4. Vorticity field for θ=120º for the three different turbulence methods

3.1. SST Results

In this section only the SST method is analysed in its several stages during a complete revolution of the rotor when a periodic solution is achieved. Fig. 5 clearly shows the several stages involved through dynamic stall for a TSR of 2.3 at different azimuth angles θ. This specific TSR was chosen because it corresponds to the case with deep stall. Fig.5 shows that for an azimuth angle θ between 180^0 and 240^0 the flow is almost attached to the blade. Then at an angle of $\theta=260^0$ a leading edge vortex will start to develop and expand until 280^0. Also, in this stage there is the generation of a trailing edge vortex that will detach at approximately 300^0. Afterwards, there is a progressive reattachment of the flow to the blade with leading and trailing edge vortices moving downstream. At $\theta=360^0$ there is again the presence of a second small leading and trailing edge vortices that will disappear between 20^0 and 40^0. Then the development of a third leading edge vortex will take place at 60^0 followed by a trailing edge vortex at 80^0. Finally, the flow will start to become laminar and to reattach to the blade until the same dynamics will start again from the beginning stage. From the final results it can be stated that the SST model shows a good agreement with the four stages related to dynamic

stall mentioned above. Furthermore, this 2-D study has the advantages of showing how the two kinds of vortices will move down and eventually affect the physics of the blades that are called to work downstream.

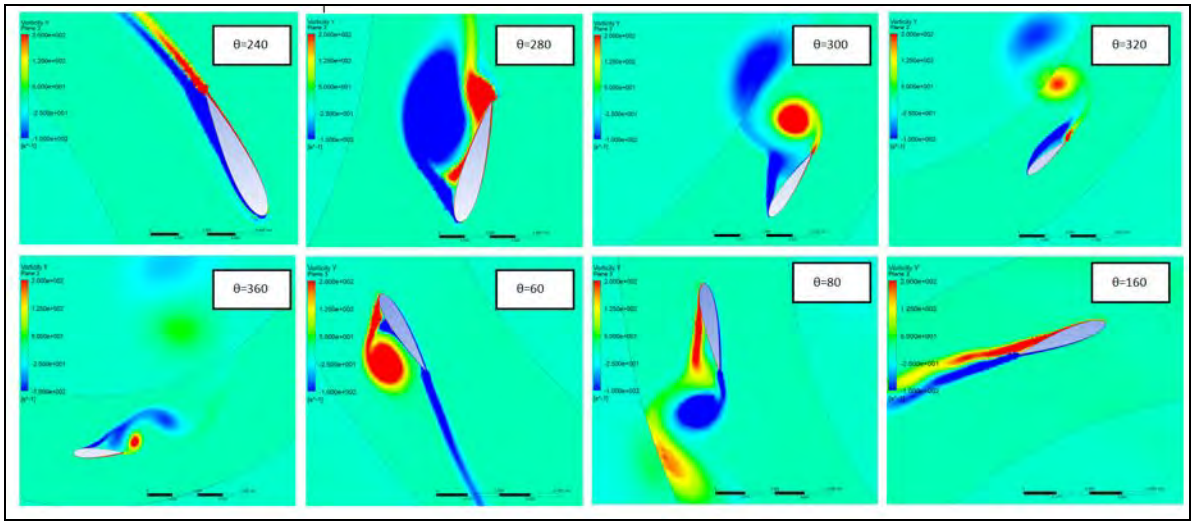

Fig. 5: Vorticity field at different azimuthal angles θ for the SST model at λ=2.3

4. Conclusions

A numerical analysis of the physics involved during dynamic stall of a rotor of a straight-bladed VAWT, composed of 3 bl ades with profile NACA0018, was conducted at four different TSRs. In this study three RANS turbulence models have been explored for the four cases analysed. The lift and drag coefficients are in good agreement with the study carried by Wang et al, but a number of differences have been found between the two studies. The most relevant are the absence of a second peak on the curves due to the development of the trailing edge vortex and the lack of intersection points at high TSRs. But at low TSRs there is an increase in the number of intersection points especially for negative angles of attacks that can be related to deep dynamic stall. This instability is mainly associated with the development of upstream wakes from upstream blades and mast that interact with the downstream blades. In this numerical study, the analysis has proved the presence of two different phenomena called dynamic and static stall that are highly depended on the TSRs adopted. In here the SST model is examined in terms of vorticity distributions around the blades. In general the method shows more reasonable accuracy with some existing wind tunnel experiments than the k-ε and k-ω turbulence methods that seem to be more dissipative. Also, the method is able to show the main four phases involved during dynamic stall. But one important observation for the SST method is the presence of single-vortices instead of having several small vortices that are typically found around the airfoil for PIV dynamic stall tests. A better improvement can be achieved in the future investigation of a 3-D case where the LES and the DES methods are strongly recommended. The two methods will take into consideration the 3-D nature of the vortices developed during dynamic stall. In general this paper gives a substantial contribution to the aerodynamics involved at different TSRs and angles of attack for a 2-D rotor with central mast. This is necessary because the development of dynamic stall in VAWTs can have a substantial impact on both the design and power generation of a wind turbine.

References

[1] K. Pope et al., Effects of stator vanes on power coefficients of a zephyr vertical axis wind

turbine, Renewable Energy, 2009, pp. 1-9.

[2] J. Knight, Urban wind power: Breezing into town, Nature, vol. 430, no. 6995, 2004, pp. 12-13.

[3] S. Mertens, Wind energy in the built environment: concentrator effects of buildings. TU Delft, 2006, pp. 3-14.

[4] R. Howell, N. Qin, J. Edwards, and N. Durrani, Wind tunnel and numerical study of a small vertical axis wind turbine, Renewable Energy, vol. 35, 2010, no.2, pp. 412-422.

[5] A. Mewburn-Crook, The Design and development of an augmented vertical wind turbine, School of Mechanical, Aeronatical and Production Engineering, 1990, pp. 1-59

[6] S. Stankovic, N. Campbell, and A. Harries, Urban Wind Energy. Earthscan, 2009.

[7] C. J. Ferreira, G. van Bussel, and G. van Kuik, 2D CFD simulation of dynamic stall on a Vertical Axis Wind Turbine: verification and validation with PIV measurements, presented at the 45th AIAA Aerospace Sciences Meeting and Exhibit, 2007, pp. 1-11.

[8] C. Hofemann, C. J. Simao Ferreira, G. J. Van Bussel, G. A. Van Kuik, F. Scarano, and K. R. Dixon, 3D Stereo PIV study of tip vortex evolution on a VAWT, 2008, pp. 1-8.

[9] G. Marsh and S. Peace, Tilting at windmills: Utility-scale VAWTs: towards 10MW and beyond? , Refocus, vol. 6, no. 5, 2005, pp. 37-42.

[10] G. Marsh, Wind turbines: How big can they get? , Refocus, vol. 6, no. 2, 2005. , pp. 22-28.

[11] C. J. Simão Ferreira, A. van Zuijlen, H. Bijl, G. van Bussel, and G. van Kuik, Simulating dynamic stall in a two-dimensional vertical-axis wind turbine: verification and validation with particle image velocimetry data, Wind Energy, vol. 13, no. 1, 2010, pp. 1-17.

[12] ANSYS Meshing: Application Introduction, ANSYS, 2009.

[13] N. Fujisawa and S. Shibuya, "Observations of dynamic stall on Darrieus wind turbine blades," Journal of Wind Engineering and Industrial Aerodynamics, vol. 89, no. 2, 2001, pp. 201-214.

[14] J. Larsen, S. Nielsen, and S. Krenk, Dynamic stall model for wind turbine airfoils, Journal of Fluids and Structures, vol. 23, no. 7, 2007, pp. 959-982.

[15] J. A. Ekaterinaris and M. F. Platzer, Computational prediction of airfoil dynamic stall, Progress in Aerospace Sciences, vol. 33, no. 11, 1998, pp. 759-846.

[16] S. Wang, D. B. Ingham, L. Ma, M. Pourkashanian, and Z. Tao, Numerical investigations on dynamic stall of low Reynolds number flow around oscillating airfoils, Computers & Fluids, vol. 39, no. 9, 2010, pp. 1529-1541.

[17] D. C. Wilcox, Turbulence Modeling for CFD. DCW industries La Canada, 2006.

[18] T. Lee and P. Gerontakos, Investigation of flow over an oscillating airfoil, Journal of Fluid Mechanics, vol. 512, 2004, pp. 313-341.

[19] C. J. Simão Ferreira, A. van Zuijlen, H. Bijl, G. van Bussel, and G. van Kuik, Simulating dynamic stall in a two-dimensional vertical-axis wind turbine: verification and validation with particle image velocimetry data, Wind Energy, vol. 13, no. 1, 2010, pp. 1-17.